ON STABILITY AND CONVERGENCE OF PROJECTION METHODS BASED ON PRESSURE POISSON EQUATION

J.-L. GUERMOND[a],* AND L. QUARTAPELLE[b]

[a] *Laboratoire d'Informatique pour la Mécanique et les Sciences de l'Ingénieur, CNRS, BP 133, 91403 Orsay, France*
[b] *Dipartimento di Fisica, Politecnico di Milano, Piazza Leonardo da Vinci, 32, 20133 Milano, Italy*

SUMMARY

This work investigates the proper choices of spatial approximations for velocity and pressure in fractional-step projection methods. Numerical results obtained with classical finite element interpolations are presented. These tests confirm the role of the *inf–sup* LBB condition in non-incremental and incremental versions of the method for computing viscous incompressible flows. © 1998 John Wiley & Sons, Ltd.

KEY WORDS: Incompressible Navier–Stokes equations; projection method; fractional-step method; pressure Poisson equation; finite elements; stabilization methods

1. INTRODUCTION

Recent investigations on the approximation of the primitive variable Navier–Stokes equations by finite elements are centered on establishing the correct interpolation for velocity and pressure unknowns. In fact, the mathematical analysis of the Stokes problem shows that the approximation spaces for velocity and pressure must *a priori* satisfy a compatibility condition known as the *inf–sup* condition and also referred to in the literature as the LBB condition by Ladyzhenskaya [14], Babŭska [1], and Brezzi [2]. The numerical consequence of not satisfying this condition often appears as severe node-to-node spatial oscillations in the pressure field, usually termed 'spurious pressure modes' by the investigators. To eliminate these unphysical features and obtain non-oscillatory numerical solutions, artificial higher-order differential terms proportional to the equation residual can be added to the discrete equation(s), giving a stablized version of the original algorithm; see for instance the works of Hughes *et al*. [13] or Tezduyar [19]. The reader is referred to Quarteroni and Valli for a review on these techniques [15].

In recent years, the idea has emerged in the literature that the Poisson-based projection techniques, as introduced by Chorin [4,5] and Temam [18], can be used with spatial interpolations which do not satisfy the LBB condition and that this kind of method falls into the class of stabilization techniques. It is the goal of the present paper to investigate this idea. More precisely the following questions are addressed:

---

* Correspondence to: Laboratoire d'Informatique pour la Mécanique et les Sciences de l'Ingénieur, CNRS, BP 133, 91403, Orsay, France. E-mail: guermond@limsi.fr

- Can equal-order interpolations be used in fractional-step projection methods based on a Poisson equation for pressure? Is the LBB condition indeed necessary for these methods?
- What are the differences in terms of stabilization and convergence properties between the non-incremental and incremental versions of the projection method?

Stated in other words, this study will investigate which combinations of space and time discretizations can be used safely in fractional-step projection methods. This requires the identification and characterization *a priori* of the projection algorithms which avoid the aforementioned spurious pressure modes by construction, rather than attempting to suppress them *a posteriori* with suitable stabilization techniques. It will be shown that this goal can be achieved while working within the theoretical framework recently proposed by the first author [9,8] for the analysis of fully discrete projection schemes (see also [11]).

The paper is structured as follows. First, the Navier–Stokes problem is stated and some notation is introduced. In Section 2, the non-incremental fractional-step method as originally proposed by Chorin [4,5] and Temam [18] is reviewed. As soon as a clear and explicit distinction is made between the vector spaces to which the intermediate and end-of-step velocities belong, the incompressible projection step is interpreted as a Poisson problem. The final algorithm is, however, formulated in terms of only one velocity field. Some numerical results are given to compare the stability and accuracy of equal-order and unequal-order interpolations. Section 3 describes an incremental version of the projection method (called also pressure correction method) which relies on the same variational framework as that of the non-incremental scheme. The stability and accuracy of the incremental method are also illustrated by numerical examples. The major conclusions of this work are reported in Section 4.

Hereafter, the main concern is the time-dependent incompressible Navier–Stokes equations formulated in terms of the primitive variables: velocity $\boldsymbol{u}$ and pressure p. The fluid domain Ω is assumed to be bounded and connected in two or three dimensions. The complete mathematical statement of the problem is: Find $\boldsymbol{u}$ and p (up to a constant) so that

$$\begin{cases} \dfrac{\partial \boldsymbol{u}}{\partial t} - v\nabla^2\boldsymbol{u} + (\boldsymbol{u}\cdot\nabla)\boldsymbol{u} + \nabla p = \boldsymbol{f}, \\[2mm] \nabla\cdot\boldsymbol{u} = \boldsymbol{0}, \\[1mm] \boldsymbol{u}|_{\partial\Omega} = \boldsymbol{b}, \\[1mm] \boldsymbol{u}|_{t=0} = \boldsymbol{u}_0, \end{cases} \tag{1.1}$$

where v is the viscosity, $\boldsymbol{f}$ is a known body force, $\boldsymbol{b}$ is the velocity prescribed on the boundary $\partial\Omega$, and $\boldsymbol{u}_0$ is the divergence-free initial velocity field. The boundary and data are assumed to be regular and to satisfy all the compatibility conditions needed for a smooth solution to exist for all time. For simplicity, only a Dirichlet boundary condition for velocity is considered here, but more general boundary conditions can be handled using the techniques presented below (see [12]).

2. THE (NON-INCREMENTAL) FRACTIONAL-STEP ALGORITHM

2.1. Time discretization

For the sake of completeness, in this section some results established in previous studies [9,12] are briefly restated and the necessary notations are introduced. Particular attention is

paid to the structural (functional analytic) difference existing between two substeps of the method, namely the viscous step and the projection step. This distinction leads to the consideration of two different vector spaces for approximating the intermediate velocity and the end-of-step velocity in the projection method.

The original fractional-step projection algorithm proposed by Chorin [4,5] and Temam [18] can be put in the following form: Set $\boldsymbol{u}^0 = \boldsymbol{u}_0$, then for $k \geq 0$, solve

$$\begin{cases} \dfrac{\boldsymbol{u}^{k+1} - i^t \hat{\boldsymbol{u}}^k}{\Delta t} - \nu \nabla^2 \boldsymbol{u}^{k+1} + (\boldsymbol{u}^k \cdot \nabla)\boldsymbol{u}^{k+1} = \boldsymbol{f}^{k+1}, \\ \boldsymbol{u}^{k+1}{}_{|\partial\Omega} = \boldsymbol{b}^{k+1}, \end{cases} \tag{2.1}$$

and

$$\begin{cases} \dfrac{\hat{\boldsymbol{u}}^{k+1} - i\boldsymbol{u}^{k+1}}{\Delta t} + \hat{\boldsymbol{\nabla}} p^{k+1} = 0, \\ \hat{\boldsymbol{\nabla}} \cdot \hat{\boldsymbol{u}}^{k+1} = 0, \\ \boldsymbol{n} \cdot \hat{\boldsymbol{u}}^{k+1}{}_{|\partial\Omega} = \boldsymbol{n} \cdot \boldsymbol{b}^{k+1}. \end{cases} \tag{2.2}$$

It is important to note the structural difference existing between the viscous step (2.1) and the projection phase (2.2) of the calculation. The first half-step constitutes an elliptic boundary value problem for an intermediate velocity $\boldsymbol{u}^{k+1}$, accounting for viscosity and convection. The second half-step represents an essentially inviscid problem which determines the end-of-step divergence-free velocity field $\hat{\boldsymbol{u}}^{k+1}$ together with a suitable approximation to the pressure distribution p^{k+1}. As a consequence, boundary conditions of a different kind are imposed on the velocity fields which are calculated in the two half-steps. Accordingly, the two operators $\boldsymbol{\nabla}\cdot$ and $\hat{\boldsymbol{\nabla}}\cdot$ occurring in the two steps are distinct, because they act on vector fields belonging to spaces which are endowed with very different regularities, namely, $\boldsymbol{H}^1$ and $\boldsymbol{H}^{\mathrm{div}}$ (or possibly $\boldsymbol{L}^2$), respectively.

The presence of two velocity spaces requires the introduction of the injection operators i: $\boldsymbol{H}_0^1 \to \boldsymbol{H}_0^{\mathrm{div}}$ and its transpose i^t, [8,9]. Roughly speaking the injection operator i performs the transfer from one velocity space to the other. Indeed, $\hat{\boldsymbol{\nabla}}\cdot\colon \boldsymbol{H}_0^{\mathrm{div}} \to L^2$ is an extension of $\boldsymbol{\nabla}\cdot\colon \boldsymbol{H}_0^1 \to L^2$ in the sense that we have the remarkable property:

$$\hat{\boldsymbol{\nabla}}\cdot i = \boldsymbol{\nabla}\cdot \quad \text{and} \quad i^t\hat{\boldsymbol{\nabla}} = \boldsymbol{\nabla}.$$

This distinction may seem unduly pedantic in the context of the spatially continuous problem, but it proves to be of the utmost importance when it comes to discretizing the equations in space.

By applying the divergence operator $\hat{\boldsymbol{\nabla}}\cdot$ to the first equation in (2.2) and by denoting $\hat{\boldsymbol{\nabla}}^2 = \hat{\boldsymbol{\nabla}}\cdot\hat{\boldsymbol{\nabla}}$ we obtain the following Poisson problem:

$$\begin{cases} -\hat{\boldsymbol{\nabla}}^2 p^{k+1} = -(\Delta t)^{-1}\hat{\boldsymbol{\nabla}}\cdot(i\boldsymbol{u}^{k+1}), \\ (\partial p^{k+1}/\partial n)_{|\partial\Omega} = 0. \end{cases} \tag{2.3}$$

Once p^{k+1} is known, the end-of-step velocity is given by the explicit relation

$$\hat{\boldsymbol{u}}^{k+1} = i\boldsymbol{u}^{k+1} - \Delta t\,\hat{\boldsymbol{\nabla}} p^{k+1}.$$

Note that, insofar as the pressure solution of the Poisson equation is in H^1, $\hat{\boldsymbol{\nabla}} p^{k+1}$ is expected to belong to $\boldsymbol{L}^2$; as a result, $\hat{\boldsymbol{u}}^{k+1}$ should *not* be expected *a priori* to have more regularity than that of $\boldsymbol{H}^{\mathrm{div}}$ (which is lower than that of $\boldsymbol{H}^1$).

The time integration scheme chosen in the momentum equation is fully implicit for the viscous term and semi-implicit for the advection term. To guarantee unconditional stability,

i.e. to avoid any restriction on the time step Δt, the advection term $(\boldsymbol{v} \cdot \boldsymbol{\nabla})\boldsymbol{u}$ is replaced hereafter by its well known skew-symmetric form $(\boldsymbol{v} \cdot \boldsymbol{\nabla})\boldsymbol{u} + 1/2\,(\boldsymbol{\nabla} \cdot \boldsymbol{v})\boldsymbol{u}$, see e.g. Temam [17] or Quarteroni and Valli [15]. Note that, since the skew-symmetry of the advection term relies on the fact that $\boldsymbol{v}$ is divergence free, one could imagine using $\hat{\boldsymbol{u}}^k$ as the advection field and writing the advection term in the form $(\hat{\boldsymbol{u}}^k \cdot \boldsymbol{\nabla})\boldsymbol{u}^{k+1}$, because $\hat{\boldsymbol{u}}^k$ is divergence free. In fact, this form is not natural because the theoretical analysis shows that $\hat{\boldsymbol{u}}$ is not regular enough for $(\hat{\boldsymbol{u}}^k \cdot \boldsymbol{\nabla})\boldsymbol{u}^{k+1}$ to be controlled by means of the usual Sobolev inequalities. This theoretical remark leads quite naturally to the formulation of the simplest projection method, with the end-of-step velocity eliminated from the final algorithm, as shown below.

2.2. Elimination of the end-of-step velocity

Indeed, the final velocity $\hat{\boldsymbol{u}}^{k+1}$ can be completely eliminated from the fractional-step algorithm, by substituting its above expression into the equation of the (next) viscous step, since we have

$$i^t\hat{\boldsymbol{u}}^k = i^t(i\boldsymbol{u}^k - \Delta t\hat{\boldsymbol{\nabla}}p^k) = i^ti\boldsymbol{u}^k - \Delta t i^t(\hat{\boldsymbol{\nabla}}p^k) = \boldsymbol{u}^k - \Delta t\boldsymbol{\nabla}p^k,$$

where we have made use of the property $i^t\hat{\boldsymbol{\nabla}} = \boldsymbol{\nabla}$. This argument is purely formal here but plays a fundamental role in the spatially discrete case. By virtue of this result, the viscous step problem can be rewritten in the simpler, but strictly equivalent, form:

$$\begin{cases} \dfrac{\boldsymbol{u}^{k+1} - \boldsymbol{u}^k}{\Delta t} - \nu\nabla^2\boldsymbol{u}^{k+1} + (\boldsymbol{u}^k \cdot \boldsymbol{\nabla})\boldsymbol{u}^{k+1} + \dfrac{1}{2}(\boldsymbol{\nabla} \cdot \boldsymbol{u}^k)\boldsymbol{u}^{k+1} = \boldsymbol{f}^{k+1} - \boldsymbol{\nabla}p^k, \\ \boldsymbol{u}^{k+1}_{|\partial\Omega} = \boldsymbol{b}^{k+1}. \end{cases} \quad (2.4)$$

2.3. Fully discretized equations

The finite element approximation $X_{0,h} \subset \boldsymbol{H}_0^1$ for the intermediate velocity $\boldsymbol{u}_h$, and $N_h \subset H_1$ for the pressure p_h are now introduced, with each pressure field being defined up to a constant. Let the polynomial order of interpolation for the velocity be denoted by $\ell(\geq 1)$ and that for the pressure by ℓ', with $\max(\ell - 1, 1) \leq \ell' \leq \ell$.

The weak variational formulation of the advection–diffusion step (2.4) is obtained straightforwardly [12], and reads:

For $k \geq 0$, find $\boldsymbol{u}_h^{k+1} \in X_{\boldsymbol{b}^{k+1},h}$ such that, for all $\boldsymbol{v}_h \in X_{0,h}$,

$$\left(\dfrac{\boldsymbol{u}_h^{k+1} - \boldsymbol{u}_h^k}{\Delta t}, \boldsymbol{v}_h\right) + \nu(\boldsymbol{\nabla}\boldsymbol{u}_h^{k+1}, \boldsymbol{\nabla}\boldsymbol{v}_h) + ((\boldsymbol{u}_h^k \cdot \boldsymbol{\nabla})\boldsymbol{u}_h^{k+1}, \boldsymbol{v}_h) + \dfrac{1}{2}(\boldsymbol{\nabla} \cdot \boldsymbol{u}_h^k, \boldsymbol{u}_h^{k+1} \cdot \boldsymbol{v}_h)$$

$$= (\boldsymbol{f}^{k+1}, \boldsymbol{v}_h) - (\boldsymbol{\nabla}p_h^k, \boldsymbol{v}_h), \quad (2.5)$$

where p_h^0 is conventionally set to zero and u_h^0 is an approximation of u_0 in $X_{\boldsymbol{b}^0,h}$. It is well-known that the skew-symmetric form of the advection term does not contribute to the kinetic energy of the approximate solution, irrespective of the value of Δt. It should also be noted that the extra term is of the order of the consistency error, due to the fact that the velocity $\boldsymbol{u}_h^{k+1}$ tends to the exact solenoidal velocity as $h \rightarrow 0$.

The projection step has a unique expression when the functional space for the end-of-step velocity is chosen. Many options are possible [8,9]; one of the simplest consists of selecting $\hat{\boldsymbol{u}}_h^{k+1}$ in $X_h + \boldsymbol{\nabla}N_h$. Given this particular choice, it can be proven that the operator $\hat{\boldsymbol{\nabla}}_h$, the discrete counterpart of $\hat{\boldsymbol{\nabla}}$, coincides exactly with the restriction of the gradient operator to N_h (in terms of distributions); as a result, the projection step takes the following form:

For $k \geq 0$, find $p_h^{k+1} \in N_h$ such that, for all $q_h \in N_h$,

$$(\nabla p_h^{k+1}, \nabla q_h) = -(\Delta t)^{-1}(\nabla \cdot \boldsymbol{u}_h^{k+1}, q_h). \tag{2.6}$$

It must be emphasized that a basic aspect of the method is the introduction of *two different* spaces to represent the velocity computed in each of the two (half-)steps of the method. In fact, the discrete velocity field provided by the projection step belongs to a space of vector functions $(X_h + \nabla N_h)$ which are discontinuous at the interfaces of the finite elements. More precisely, the normal component of the end-of-step velocity $\hat{\boldsymbol{u}}^{k+1}$ is discontinuous at the interfaces between the (pressure) elements. Although this choice may seem peculiar, it is the most natural in the context of projection schemes based on the Poisson equation for pressure. On the other hand, the discrete end-of-step velocity is never explicitly referenced in the numerical algorithm, which is formulated in terms of the intermediate velocity only.

Other choices of the functional space for the end-of-step velocity are possible. For instance, Gresho and Chan [7] used $\hat{\boldsymbol{u}}_h^{k+1}$ in $X_{\boldsymbol{b}^{k+1},h}$. This choice is permitted, provided that the LBB condition between X_h and N_h is satisfied; however, it is not optimal and yields a discrete problem for the pressure involving the inverse of the mass matrix. The reader is referred to Reference [9] for a review of other possible choices.

2.4. Stability and convergence

The stability and convergence properties of the non-incremental projection scheme, (2.5) and (2.6), will now be discussed. The incompressibility constraint is enforced through an *uncoupled* pressure Poisson problem, therefore, it may appear that in principle any spatial discretization for approximating elliptic problems is admissible. It is the goal of this section to show that this impression is partially false.

One remarkable feature of the non-incremental scheme is a type of intrinsic stability of the pressure solution, irrespective of the satisfaction of any *inf–sup* condition between the velocity space X_h and the pressure space N_h. More precisely, from (2.6) it is inferred that the H^1 norm $\|p_h^{k+1}\|_1$ is bounded by the L^2 norm $(\Delta t)^{-1}\|\boldsymbol{u}_h^{k+1} - \boldsymbol{u}(t^{k+1})\|_0$. Using arguments similar to that of Rannacher [16], one can infer that $(\Delta t)^{-1}\|\boldsymbol{u}_h^{k+1} - \boldsymbol{u}(t^{k+1})\|_0$ is bounded by

$$\frac{c(\Delta t + h^{\ell+1})}{\Delta t} = c(1 + h^{\ell+1}/\Delta t).$$

From this it can be inferred that, if $\Delta t \geq ch^{\ell+1}$, then the pressure satisfies the following *stability* estimate:

$$\max_{1 \leq k \leq K} \|p_h^{k+1}\|_1 \leq c.$$

This condition means that any H^1-conformal interpolation yields a stable approximation of the pressure, provided Δt is not too small, namely,

$$\Delta t \geq ch^{\ell+1}.$$

For instance, an equal-order interpolation, e.g. P_1/P_1 elements is permitted if Δt is not too small in the sense specified above. Of course, Δt is not subject to any stability restriction whenever X_h and N_h satisfy the LBB condition.

On the other hand, when it comes to the convergence analysis, the LBB condition also seems to be necessary to establish error estimates. By extending Rannacher's arguments to the spatially discrete problem, it can be shown that, provided the LBB condition is satisfied,

$$\max_{0 \leq k \leq K} \|\boldsymbol{u}_h^k - \boldsymbol{u}(t^k)\|_0 + \max_{0 \leq k \leq K} \|\hat{\boldsymbol{u}}_h^k - \boldsymbol{u}(t^k)\|_0 \leq c[\boldsymbol{u}, p](\sqrt{\Delta t} + h^{\ell+1}), \tag{2.7}$$

$$\max_{0 \leq k \leq K} \|\boldsymbol{u}_h^k - \boldsymbol{u}(t^k)\|_1 + \max_{0 \leq k \leq K} \|p_h^k - p(t^k)\|_0 \leq c[\boldsymbol{u}, p](\sqrt{\Delta t} + h^{\ell}). \tag{2.8}$$

It is not known to the authors whether such estimates can be obtained without the LBB assumption. However, the numerical results shown in Section 2.5 provide a clear indication that no convergence estimate (on the pressure and velocity) seems possible if the condition $\Delta t \geq ch^{\ell + 1}$ is violated.

The first estimate (2.7) can be further refined by making use of sophisticated duality arguments [16] to give

$$\max_{0 \leq k \leq K} \|u_h^k - u(t^k)\|_0 + \max_{0 \leq k \leq K} \|\hat{u}_h^k - u(t^k)\|_0 \leq c[u, p](\Delta t + h^{\ell + 1}). \tag{2.9}$$

This improvement does not apply to the H^1 norm of the velocity or the L^2 norm of the pressure as a consequence of the presence of a numerical boundary layer (see Rannacher [16]). Such a limitation on the accuracy in the H^1 norm is a particular feature of the non-incremental method as compared with the incremental one which will be described in Section 3.

2.5. Numerical results

For the numerical illustrations we rely upon the well-known standard driven cavity problem [3]. A Reynolds number equal to 100, which is well documented in the literature, is used. All the linear systems involved in the algorithm are solved by direct methods for large sparse systems of linear equations. Note that the unconditionally stable semi-implicit scheme guarantees that the tests do not suffer from the instabilities usually induced by large convection terms when made explicit. To emphasize the effect of not respecting the LBB condition, the calculations are performed on uniform meshes.

First, the non-incremental method with an equal-order P_1/P_1 interpolation is considered, using a mesh of 2×40^2 equal triangles. The steady state pressure fields computed with two representative time steps $\Delta t = 0.1$ and 0.01 are shown in Figure 1. The rather strong sensitivity of the steady solution to the value of Δt used in the computation is clearly seen. In both cases $\Delta t \geq ch^2$, therefore, the solution is smooth and no spurious pressure modes appear.

However, this does not mean that they are not present. In fact, when the same driven cavity problem is solved using $\Delta t \leq ch^2$, e.g. $\Delta t = 0.0001$, the pressure and velocity solutions show wild spatial oscillations as depicted in Figure 2, for instance, for the solution after 200 time
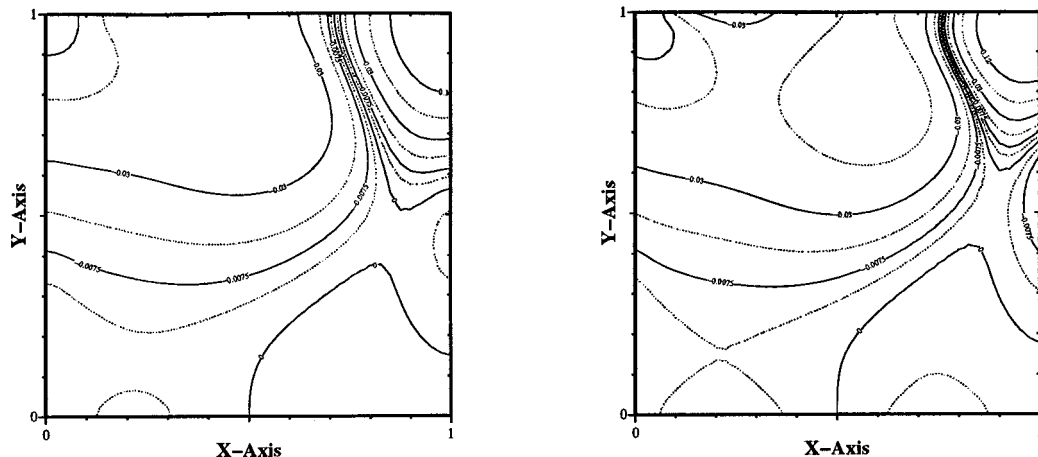

Figure 1. Pressure field in the driven cavity $R = 100$: Non-incremental method with equal-order P_1/P_1 interpolation. Left $\Delta t = 0.1$ and right $\Delta t = 0.01$.
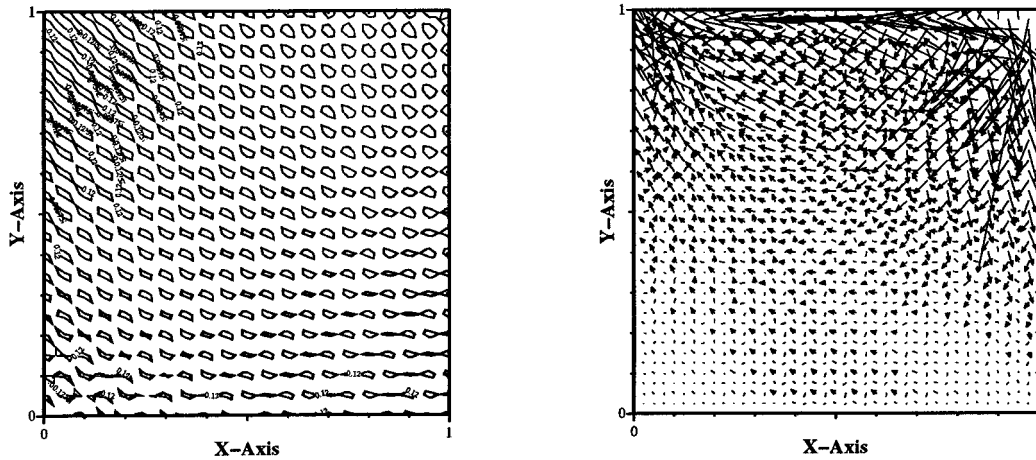
Figure 2. Pressure (left) and velocity (right) in the driven cavity $R = 100$: Non-incremental method with equal-order P_1 / P_1 interpolation. $\Delta t = 0.0001$, solution after 200 time steps.

steps. Contrary to the common believe, it is not only the pressure that is plagued but also the velocity, and it seems rather problematic to devise a method for recovering an acceptable velocity field in a post-processing phase.

To clarify whether the onset of the spatial oscillations could be caused by the corner singularities of the driven cavity problem, a simple test problem consisting of the following analytical solution in the unit square $\Omega = [0, 1]^2$ is considered:

$$\begin{cases} u_x = -g(t) \cos x \sin y, \\ u_y = g(t) \sin x \cos y, \\ p = -\frac{1}{4}[\cos(2x) + \cos(2y)]g^2(t), \end{cases}$$

where $g(t) = \sin(2t)$. If the velocity is put in the formal form $\boldsymbol{u} = \bar{\boldsymbol{u}}(x, y)g(t)$, then the source term corresponding to the Navier–Stokes equations is $\boldsymbol{f} = \bar{\boldsymbol{u}}(x, y)[g'(t) + 2g(t)/R]$. This problem is solved on two P_1/P_1 meshes consisting of 2×10^2 and 2×20^2 equal triangles, respectively. The Reynolds number R is set to 100; the pressure field computed on the coarse mesh with $\Delta t = 0.0001$ after 1000 time steps and the pressure field obtained on the fine mesh with $\Delta t = 0.00001$ after 10 000 time steps are reported in Figure 3. Wild spatial oscillations on the pressure are present also in this smooth problem. These results confirm that the time step restriction is necessary to avoid the development of the spurious modes in the discrete solution.

The conclusion of these tests is that using time steps 'sufficiently' large can hide the necessity of satisfying the LBB condition in non-incremental fractional-step projection methods. Stated alternatively, the non-incremental projection method may work well with equal-order interpolations, only if the time step is chosen to satisfy the unexpected 'inverse' stability condition $\Delta t \geq ch^{\ell + 1}$.

To verify the error estimate (2.9), we carried out a convergence test with respect to Δt using a P_1/P_1 mesh fine enough, 2×40^2, so that the spatial error is much smaller than the
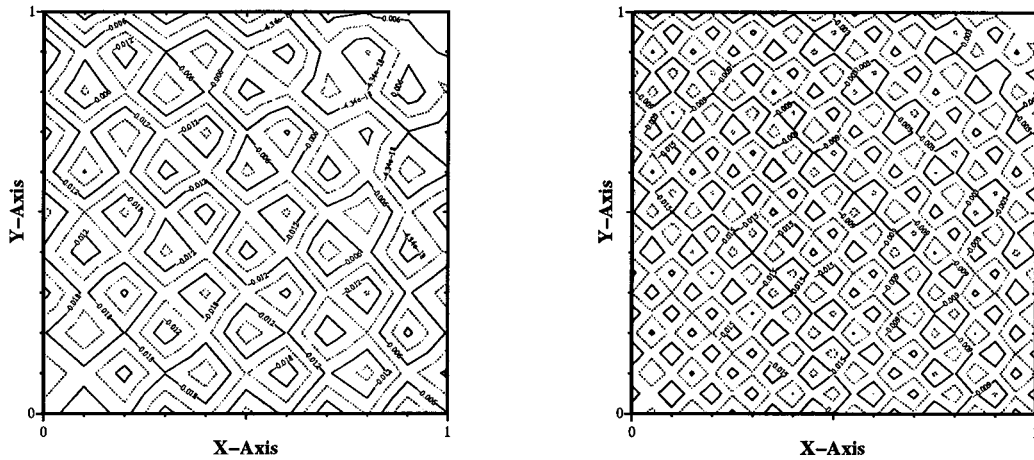
Figure 3. Pressure fields in the analytical test problem for $R = 100$: Non-incremental method with equal-order P_1/P_1 interpolation. Left: $\Delta t = 0.0001$, solution after 1000 time steps on a 2×10^2 mesh. Right: $\Delta t = 0.00001$, solution after 10 000 time steps on a 2×20^2 mesh.

temporal one. The maximum in time of the L^2 norm of the error on the velocity and the error on the pressure, for $0 \le t \le 6$, i.e. $l^{\infty}(0, 6; L^2)$, are reported in Figure 4. Both the error on the pressure and the velocity show a first-order convergence rate (always assuming that $\Delta t \ge ch^2$).

2.6. A simple stabilization of the non-incremental scheme

Since the instability of the non-incremental method occurs only for very small time steps, an elementary way of circumventing this difficulty consists of replacing Δt in the projection step with $\Delta t_{\text{stab}} = \Delta t + h_{\text{max}}^{\ell+1}$, where h_{max}, is the maximum size of the elements. The time step, Δt, in the advection diffusion phase remains unchanged. This most simple stabilization technique has been numerically verified by the authors to be effective.
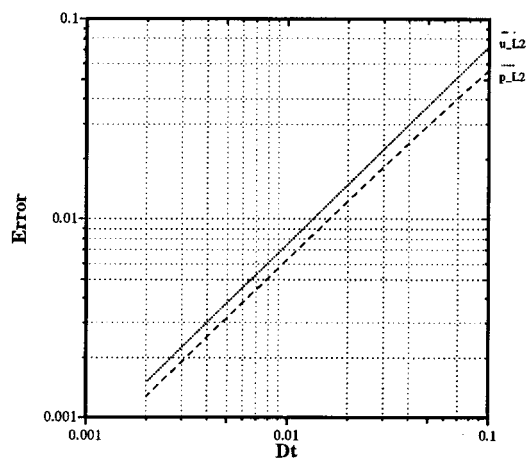

Figure 4. Convergence tests for the non-incremental projection method, with equal-order P_1/P_1 interpolation. Analytical test problem for $R = 100$, finite element mesh 2×40^2.

3. THE INCREMENTAL FRACTIONAL-STEP ALGORITHM

An incremental version of the projection method, seemingly first proposed by Goda [6] is now considered. The theoretical analysis of this scheme was performed by Guermond and Quartapelle [11]. The aim of this section is to show that the distinction between the two velocity functional spaces still plays a key role in the convergence analysis of the method, as well as in its practical implementation. Furthermore, the incremental method is shown hereafter to be more accurate than the non-incremental one for any value of the time step, the price to be paid for such a greater accuracy being the fulfilment of the LBB condition, though *a priori* this condition may not appear to be necessary.

3.1. Time discretization

The incremental version of the fractional-step method consists of making the pressure at the viscous step explicit and correcting it at the projection step, while still retaining the complete uncoupling of viscous diffusion from incompressibility.

Setting $\boldsymbol{u}^0 = \boldsymbol{u}_0$ and assuming p^0 to be known, for $k \geq 0$ solve the following two problems: First, consider the advection–diffusion step

$$\begin{cases} \dfrac{\boldsymbol{u}^{k+1} - i^t \hat{\boldsymbol{u}}^k}{\Delta t} - v\nabla^2 \boldsymbol{u}^{k+1} + (\boldsymbol{u}^k \cdot \boldsymbol{\nabla})\boldsymbol{u}^{k+1} + \dfrac{1}{2}(\boldsymbol{\nabla} \cdot \boldsymbol{u}^k)\boldsymbol{u}^{k+1} = \boldsymbol{f}^{k+1} - \boldsymbol{\nabla}p^k, \\ \boldsymbol{u}^{k+1}|_{\partial\Omega} = \boldsymbol{b}^{k+1}; \end{cases} \tag{3.1}$$

then, perform the projection step in the following incremental (correction) form:

$$\begin{cases} \dfrac{\hat{\boldsymbol{u}}^{k+1} - i\boldsymbol{u}^{k+1}}{\Delta t} + \hat{\boldsymbol{\nabla}}(p^{k+1} - p^k) = 0, \\ \hat{\boldsymbol{\nabla}} \cdot \hat{\boldsymbol{u}}^{k+1} = 0, \\ \boldsymbol{n} \cdot \hat{\boldsymbol{u}}^{k+1}|_{\partial\Omega} = \boldsymbol{n} \cdot \boldsymbol{b}^{k+1}, \end{cases} \tag{3.2}$$

where $\hat{\boldsymbol{\nabla}}\cdot$ is an extension of the usual divergence operator $\boldsymbol{\nabla}\cdot$, as explained previously. By applying $\hat{\boldsymbol{\nabla}}\cdot$ to the first equation of (3.2), the following Poisson equation for the pressure increment $(p^{k+1} - p^k)$ is obtained:

$$\begin{cases} -\hat{\boldsymbol{\nabla}}^2(p^{k+1} - p^k) = -(\Delta t)^{-1}\boldsymbol{\nabla} \cdot \boldsymbol{u}^{k+1}, \\ \dfrac{\partial(p^{k+1} - p^k)}{\partial n}\bigg|_{\partial\Omega} = 0, \end{cases} \tag{3.3}$$

where $\hat{\boldsymbol{\nabla}} \cdot i = \boldsymbol{\nabla}\cdot$.

Similar to the non-incremental scheme, the end-of-step velocity is eliminated by using the relation

$$i^t\hat{\boldsymbol{u}}^k = i^t[i\boldsymbol{u}^k - \Delta t\hat{\boldsymbol{\nabla}}(p^k - p^{k-1})] = i^t i\boldsymbol{u}^k - \Delta t i^t[\hat{\boldsymbol{\nabla}}(p^k - p^{k-1})] = \boldsymbol{u}^k - \Delta t\boldsymbol{\nabla}(p^k - p^{k-1}),$$

so that the (subsequent) viscous step becomes

$$\begin{cases} \dfrac{\boldsymbol{u}^{k+1} - \boldsymbol{u}^k}{\Delta t} - v\nabla^2 \boldsymbol{u}^{k+1} + (\boldsymbol{u}^k \cdot \boldsymbol{\nabla})\boldsymbol{u}^{k+1} + \dfrac{1}{2}(\boldsymbol{\nabla} \cdot \boldsymbol{u}^k)\boldsymbol{u}^{k+1} = \boldsymbol{f}^{k+1} - \boldsymbol{\nabla}(2p^k - p^{k-1}), \\ \boldsymbol{u}^{k+1}|_{\partial\Omega} = \boldsymbol{b}^{k+1}. \end{cases} \tag{3.4}$$

3.2. Fully discretized equations

By introducing finite element spaces $X_{0,h}$ and N_h as in Section 2.3, the incremental projection algorithm is recast in the following weak form:

For $k \geq 0$, find $\boldsymbol{u}_h^{k+1} \in X_{\boldsymbol{b}^{k+1},h}$ such that, for all $\boldsymbol{v}_h \in X_{0,h}$,

$$\left(\frac{\boldsymbol{u}_h^{k+1} - \boldsymbol{u}_h^k}{\Delta t}, \boldsymbol{v}_h\right) + \nu(\nabla \boldsymbol{u}_h^{k+1}, \nabla \boldsymbol{v}_h) + ((\boldsymbol{u}_h^k \cdot \nabla)\boldsymbol{u}_h^{k+1}, \boldsymbol{v}_h) + \frac{1}{2}(\nabla \cdot \boldsymbol{u}_h^k, \boldsymbol{u}_h^{k+1} \cdot \boldsymbol{v}_h)$$

$$= (\boldsymbol{f}^{k+1}, \boldsymbol{v}_h) - (\nabla(2p_h^k - p_h^{k-1}), \boldsymbol{v}_h). \tag{3.5}$$

The intermediate velocity $\boldsymbol{u}_h^1$ at the first time step is also evaluated from Equation (3.5) where, by convention, we set $p_h^{-1} = p_h^0$.

With $X_h + \nabla N_h$ still as the functional space for the end-of-step velocity $\hat{\boldsymbol{u}}^{k+1}$, we obtain the following form of the projection step:

For $k \geq 0$, find $(p_h^{k+1} - p_h^k) \in N_h$ such that, for all $q_h \in N_h$,

$$(\nabla(p_h^{k+1} - p_h^k), \nabla q_h) = -(\Delta t)^{-1}(\nabla \cdot \boldsymbol{u}_h^{k+1}, q_h). \tag{3.6}$$

3.3. Stability and convergence

It should be noted that the two steps (3.5) and (3.6) are fully uncoupled and could be solved in principle by any H^1-conformal finite element technique without the two approximation spaces $X_{0,h}$ and N_h being subordinate to the LBB condition. Nevertheless, this view (widely shared in the literature) is false because the stability provided by the Poisson equation only applies to the pressure *increment*, whereas in the non-incremental algorithm the stability is guaranteed on the pressure itself. This feature is clearly illustrated by the numerical tests to be presented in Section 3.4.

The description of the incremental version of the fractional-step method is concluded by recalling the following result established by Guermond and Quartapelle [11].

Theorem 1: *Under convenient regularity assumptions on the data $\boldsymbol{f}$, $\boldsymbol{u}_0$, $\boldsymbol{b}$, and provided the LBB condition is satisfied, the solution to the incremental projection scheme (3.5) and (3.6) satisfies the error bounds:*

$$\max_{0 \leq k \leq K} \|\boldsymbol{u}_h^k - \boldsymbol{u}(t^k)\|_0 + \max_{0 \leq k \leq K} \|\hat{\boldsymbol{u}}_h^k - \boldsymbol{u}(t^k)\|_0 \leq c[\boldsymbol{u}, p](\Delta t + h^{\ell+1}), \tag{3.7}$$

$$\max_{0 \leq k \leq K} \|\boldsymbol{u}_h^k - \boldsymbol{u}(t^k)\|_1 + \max_{0 \leq k \leq K} \|p_h^k - p(t^k)\|_0 \leq c[\boldsymbol{u}, p](\Delta t + h^{\ell}), \tag{3.8}$$

as $\Delta t \to 0$ and $h \to 0$, where ℓ is the interpolation degree of the velocity.

These error estimates show that the incremental algorithm achieves an $\mathcal{O}(\sqrt{\Delta t})$ increase of accuracy with respect to the non-incremental algorithm. Moreover, let $(\boldsymbol{w}_h, q_h)$ denote the solution of the fully coupled problem: setting $\boldsymbol{w}_h^0 = \boldsymbol{u}_h^0$, and for $k \geq 0$, $\boldsymbol{w}_h^{k+1} \in X_{\boldsymbol{b}^{k+1},h}$ and $q_h^{k+1} \in N_h$ are defined such that,

$$\begin{cases} \left(\dfrac{\boldsymbol{w}_h^{k+1} - \boldsymbol{w}_h^k}{\Delta t}, \boldsymbol{v}_h\right) + \nu(\nabla \boldsymbol{w}_h^{k+1}, \nabla \boldsymbol{v}_h) + ((\boldsymbol{w}_h^k \cdot \nabla)\boldsymbol{w}_h^{k+1}, \boldsymbol{v}_h) + \dfrac{1}{2}(\nabla \cdot \boldsymbol{w}_h^k, \boldsymbol{w}_h^{k+1} \cdot \boldsymbol{v}_h) \\ \quad - (q_h^{k+1}, \nabla \cdot \boldsymbol{v}_h) = (\boldsymbol{f}^{k+1}, \boldsymbol{v}_h), \quad \forall \boldsymbol{v}_h \in X_{0,h}, \\ (\nabla \cdot \boldsymbol{w}_h^{k+1}, r_h) = 0, \quad \forall r_h \in N_h. \end{cases} \tag{3.9}$$

The solution of this problem can be obtained by various means; for instance, it can be calculated by solving iteratively the Uzawa operator (see *e.g.* Temam [17] for an introduction to this technique). The computational cost for evaluating the coupled solution, $(\boldsymbol{w}_h, q_h)$, is in general much higher than that needed for evaluating the uncoupled solution $(\boldsymbol{u}_h, p_h)$ of (3.5)
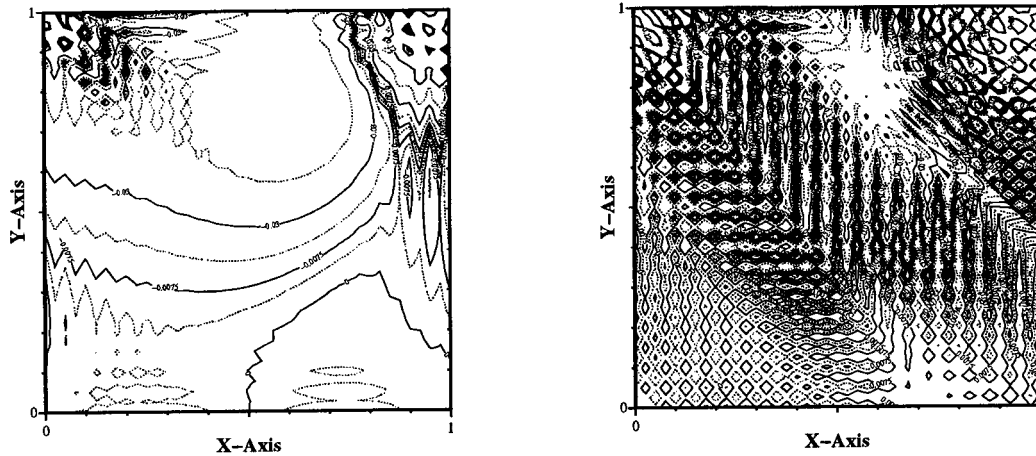
Figure 5. Pressure field in the driven cavity $R = 100$: Incremental method with equal-order P_1/P_1, interpolation. Left $\Delta t = 0.1$ and right $\Delta t = 0.01$.

and (3.6). Indeed, it is this difference in the computational costs that is at the origin of the popularity of fractional-step projection methods. The difference between w_h and u_h is the error induced by the uncoupling of the incompressibility constraint; this difference is conventionally called the time-splitting error. Guermond [10] proved that the time-splitting error induced by the incremental algorithm is indeed $\mathcal{O}((\Delta t)^2)$:

Theorem 2: *Under convenient regularity assumptions on the data f, u_0, b, and provided the LBB condition is satisfied, the solution (u_h, p_h) to the incremental projection scheme (3.5) and (3.6) satisfies the following bounds:*

$$\|u_h - w_h\|_{l^2(L^2)} + \|\hat{u}_h - w_h\|_{l^2(L^2)} \le c[u, p](\Delta t)^2 \qquad (3.10)$$

as $\Delta t \to 0$, where (w_h, q_h) is the solution to the coupled problem (3.9).

This result implies that second-order accuracy in time is possible if the first-order Euler time stepping is replaced by a second-order scheme, e.g. Crank–Nicolson or three-level backward differencing (see [10]).

3.4. Numerical results

To illustrate the necessity of satisfying the LBB condition when using the incremental projection method, the driven cavity problem is solved at $R = 100$ by the incremental algorithm using equal-order P_1/P_1 interpolation on a uniform mesh of 2×40^2 triangles. The steady state pressure fields computed with two representative time steps $\Delta t = 0.1$ and 0.01 are shown in Figure 5. Severe node-to-node oscillations clearly appear in both cases, the worst case corresponding to the smaller time step. These results confirm that the LBB compatibility condition must be satisfied for the incremental method to work properly, although the use of large time steps can make this necessity less evident.

The same calculations have been performed using a mixed P_1/P_2 method over a mesh of 2×20^2 triangles with linear interpolation for pressure and parabolic for velocity. As predicted by the theory, the steady state solution is independent of Δt. The steady pressure field is reported in Figure 6.

It must be emphasized that a refinement of the mesh for the equal-order interpolation is not capable of curing the spatial oscillations, as clearly demonstrated by Figure 7 for $\Delta t = 0.01$.
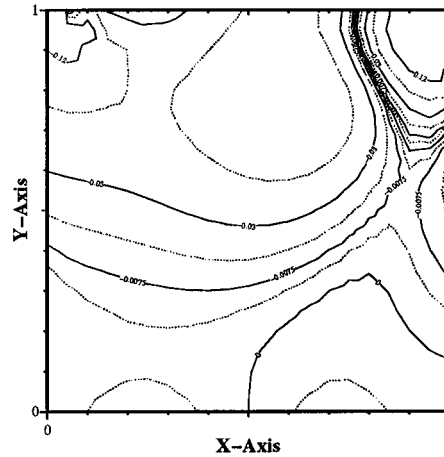
Figure 6. Steady state pressure field in the driven cavity $R = 100$: Incremental method with mixed P_1/P_2 interpolation.

Here, the solution obtained by the equal-order P_1/P_1 approximation on a mesh of 2×80^2 of equal triangles is compared with that obtained by the mixed P_1/P_2 approximation on a mesh of 2×40^2 linear/parabolic elements for pressure/velocity.

To verify the error estimates (3.7) and (3.8), convergence tests are performed on the analytical problem introduced in Section 2.5. The tests are carried out on a 2×20^2 mesh by comparing the computed solution with the Lagrange interpolation of the analytical one. The mesh is fine enough to guarantee that, on the range of time steps explored, the spatial error is much smaller than the temporal error. The $l^\infty(L^2)$ and $l^\infty(H^1)$ norms of the error on the velocity and the $l^\infty(L^2)$ norm for the error on the pressure, for $0 \leq t \leq 6$, i.e. $l^\infty(0, 6; L^2)$, are reported in Figure 8. The $l^\infty(L^2)$ norm of the error on pressure and velocity together with the $l^\infty(H^1)$ norm of the error on velocity show a first-order convergence rate as theoretically predicted.
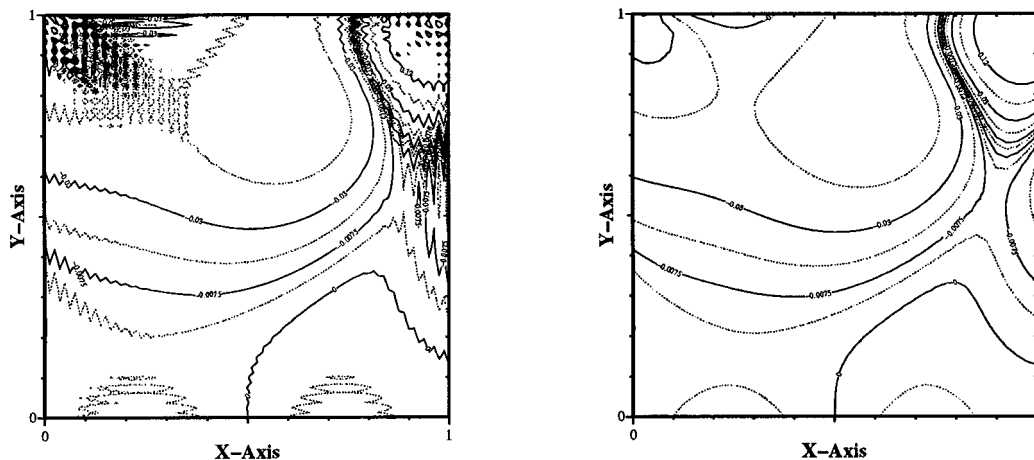

Figure 7. Pressure field in the driven cavity $R = 100$ on finer meshes: Incremental method with equal-order P_1/P_1 interpolation on a 2×80^2 mesh (left) and mixed P_1/P_2 interpolation on a 2×40^2 mesh (right); $\Delta t = 0.01$.
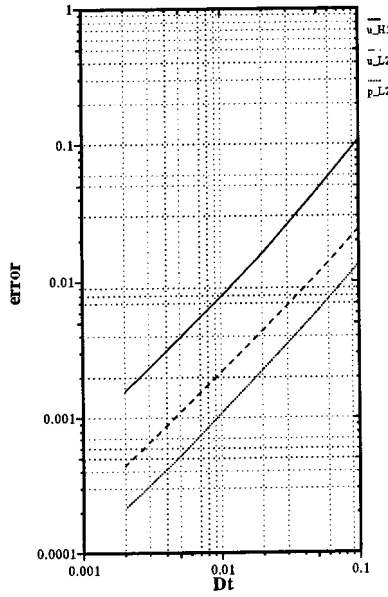
Figure 8. Convergence tests for the incremental projection method, with mixed P_1/P_2 interpolation. Analytical test problem for $R = 100$; finite element mesh 2×20^2.

To illustrate the capability of the incremental method to provide $(\Delta t)^2$ time accuracy as predicted in (3.10), convergence tests are conducted on a fixed mesh by comparing the solution calculated by the projection method with that of the coupled system (3.9) obtained by solving the Uzawa operator. The tests are performed on the driven cavity using an unstructured P_1/P_2
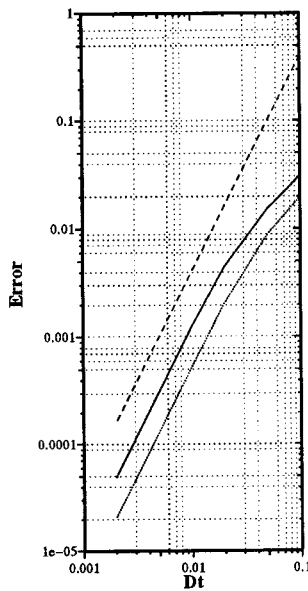

Figure 9. Convergence tests for the incremental projection method on the time regularized driven cavity; $R = 100$, with mixed P_1/P_2 interpolation. Splitting error versus time step Δt for the velocity (solid line) and pressure (dotted line); Second-order slope (dashed line).

Table I. Role of the compatibility *inf–sup* LBB condition in fractional-step projection methods

Method	Stability	Convergence
Non-incremental	Necessary, excluding when $\Delta t \geq ch^{\ell+1}$	Necessary
Incremental	Necessary (always)	Necessary

triangulation consisting of ≈ 400 P_2-nodes. To avoid a possible blow-up of the errors at the initial time, the top wall velocity has been regularized in time by prescribing the following time dependence: $U(t) = (t/\tau)^4/[1 + (t/\tau)^4]$, where $\tau = 0.2$. The regularization procedure is not necessary for the method to work (the algorithm easily accepts an impulsive start); however, it avoids irrelevant initial errors induced by the initialization procedure and ensures that initial data satisfy all the compatibility conditions required by the error analysis. With such a regularization, $p_h^{-1} = p_h^0 = 0$ and $u_h^0 = 0$ can be chosen, and the solution is clearly reasonably smooth in time.

In Figure 9, the errors on measured velocity and pressure are plotted, respectively, by the maximum in time of the energy norm, i.e. $l^\infty(0, 1; \boldsymbol{L}^2)$, for the velocity (solid line) and by the energy norm in space and time, i.e. $l^2(0, 1; L^2)$, for the pressure (dotted line). The dashed line corresponds to second-order convergence in time. The conclusion of these tests is that the present incremental scheme yields second-order time accuracy, when the error is measured by the distance of the solution from that of the coupled scheme.

This convergence test confirms the superiority of the incremental projection method (as a splitting technique) over the non-incremental one in the sense that it retains the optimal space approximation property of the finite elements, while introducing a second-order error in time when compared with the coupled method (3.9).

4. CONCLUSIONS

This paper has investigated the stability and convergence of fractional-step projection methods based on spatial discretizations by finite elements. The study was focused on projection schemes with the incompressible step recast in terms of a Poisson equation for the pressure. The analysis was conducted within a theoretical framework which assumes that the intermediate velocity and the end-of-step velocity belong to two distinct spaces of discrete vector functions, even if only one of the two appears in the final computational algorithm.

In such a context, two main points have been addressed: (1) the comparison of schemes based on non-incremental or incremental time discretization of the two half steps, and (2) the investigation of equal-order or unequal-order interpolations for pressure and velocity.

A semi-implicit unconditionally stable time integration has been used in some simple but representative model calculations to verify the predictions of the finite element theory

Table II. Stability of finite element interpolations in fractional-step projection methods

	Finite element Interpolations	
Method	Equal-order: P_1/P_1, Q_1/Q_1	Mixed methods: MINI, P_1/P_2, Q_1/Q_2
Non-incremental	Unstable, excluding when $\Delta t \geq ch^{\ell+1}$	Stable
Incremental	Unstable (always)	Stable

Table III. Irreducible time-splitting error in fractional-step projection methods

Method	Time-splitting error
Non-incremental	$\mathcal{O}(\Delta t)$
Incremental	$\mathcal{O}((\Delta t)^2)$

concerning projection schemes. The numerical results confirm that the non-incremental method has convergence properties inferior to those of the incremental one. The inferiority is related to a kind of stabilization intrinsic to the non-incremental scheme, which makes the use of interpolations of the same order for velocity and pressure possible, without the parasitic pressure mode being excited by non-linear effects, but only provided that the time step is not too small with respect to the spatial mesh size, in the sense that $\Delta t \geq ch^{\ell+1}$, ℓ being the velocity interpolation degree.

In contrast, the incremental (pressure correction) method has much better convergence properties and, in complete compliance with the well known LBB condition, must be implemented by means of interpolations of different order (mixed method) to provide a stable method for any time step. Such a method gives non-oscillatory velocity and pressure fields under ordinary circumstances, without requiring the introduction of any *ad hoc* stabilization technique.

The results provided by the theoretical and computational analysis conducted in this paper are summarized in Table I. Stated in terms of stability of some finite element interpolations, these results can be summarized as in Table II.

Finally, this work can be concluded by summarizing in Table III the highest order of the time-splitting error which can be achieved by the two versions of the projection algorithm discussed in the paper.

REFERENCES

1. I. Babŭska, *Numer. Math.*, **20**, 179–192 (1973).
2. F. Brezzi, *R.A.I.R.0.*, **R.2**, 129–151 (1974).
3. O.R. Burggraf, *J. Fluid Mech.*, **24**, 113–151 (1966).
4. A.J. Chorin, *Math. Comp.*, **22**, 745–762 (1968).
5. A.J. Chorin, *Math. Comp.*, **23**, 341–353 (1969).
6. K. Goda, *J. Comput. Phys.*, **30**, 76–95 (1979).
7. P.M. Gresho and S.T. Chan, *Int. j. numer. methods fluids*, **11**, 587–620 (1990).
8. J.-L. Guermond, *C. R. Acad. Sc. Paris, Serie I*, **319**, 887–892 (1994).
9. J.-L. Guermond, *Model. Math. Anal. Numer.*, **30**, 637–667 (1996).
10. J.-L. Guermond, 'Un résultat de convergence à l'ordre deux en temps pour l'approximation des équations de Navier–Stokes par une technique de projection', *Modél. Math. Anal. Numér. (M²AN)*, in press and LIMSI report 97-05.
11. J.-L. Guermond and L. Quartapelle, 'On the approximation of the unsteady Navier–Stokes equations by finite element projection methods', *Numer. Math.*, in press.
12. J.-L. Guermond and L. Quartapelle, *J. Comput. Phys.*, **132**, 12–33 (1997).
13. T.J.R. Hughes, L.P. Franca and M. Balestra, *Comput. Methods Appl. Mech. Eng.*, **63**, 85–99 (1986).
14. O.A. Ladyshenskaya, *The Mathematical Theory of Viscous Incompressible Flow*, 2nd edn, Gordon and Breach, New York, 1969.
15. A. Quarteroni and A. Valli, *Numerical Approximation of Partial Differential Equations*, Springer Series in Computational Mathematics, Vol. 23 Springer, Berlin, 1994.
16. R. Rannacher, *Lectures Notes in Mathematics*, 1530, Springer, Berlin, 1992, pp. 167–183.
17. R. Temam, 'Navier–Stokes Equations', *Studies in Mathematics and its Applications*, Vol. 2, North-Holland, Amsterdam, 1977.
18. R. Temam, *Bull. Soc. Math. France*, **98**, 115–152 (1968).
19. T.E. Tezduyar, S. Mittal, S.E. Ray and R. Shim, *Comput. Meths. Appl. Mech. Eng.*, **95**, 221–242 (1992).